Coastally Trapped Waves over a Double Shelf Topography(III): Forced Waves and Circulations Driven by Winds in the Yellow Sea

Ig-Chan PANG
Department of Oceanography, National University of Cheju, Cheju 690-120, Korea

The first order wave equation over a double shelf has wind stresses on both coastal boundaries and wind stress curl forcing across the shelf. In the Yellow Sea, the effect of wind stress curl can be neglected as a forcing of shelf waves. The decay distance of Kelvin waves is much greater than that of continental shelf waves so that Kelvin waves are transmitted nearly intact through the northern embayment. The numerical method of characteristics has been modified to accomodate wave propagation of opposite directions.

Using a little more realistic coastline, the wave model hindcast has been improved for current velocity, but hardly for sea level. It means that Kelvin waves, which mainly determine sea levels, are affected little by the change of bottom slope. For a better hindcast of sea level, input energy of Kelvin waves transmitted from the East China Sea is needed. The basic structure of downwind flows along the coasts and upwind flows along the trough supports the seasonal circulations driven by monsoon winds in the Yellow Sea.

Introduction

The theory of coastally trapped waves over a double shelf topography shown in the Yellow Sea has been recently studied, and based on the theory, a long wave model for the Yellow Sea has been developed and applied to reproduce some of fluctuations in sea level and current velocity observed during January to April 1986(Pang, 1987; Hsueh and Pang, 1989). The application has been successful, specially in reproducing qualitatively the upwind flow bursts in the Yellow Sea trough. The success makes the model to be used to address the dynamics of the Yellow Sea circulation. However, more processes should be added to develop the theory and the wave model. Some of them have been worked for free waves in Pang(1991, 1992) and some of them are going to be worked for forced waves in this study.

The wave equation is first derived by Gill and Schumann(1974) for a single shelf and friction is added incurring an infinite coupled set of modes by Brink and Allen(1978). The fully coupled set of wave equations is first solved by integration along the characteristics by Clarke and Van Gorder(1986). The wave equation for a double shelf is derived and solved by Pang(1987). The method of characteristics used to solve it is basically similar to that found in Clarke and VanGorder(1986), except that the integration proceeds in time increment to accomodate wave propagations to the north and south simultaneously(Clarke and VanGorder used a distance increment, which is possible for only one-directional wave propagation.) and that for a given distance in y, time increment is much smaller because Kelvin waves are included(Kelvin wave is not included in most previous shelf wave models.).

이 논문은 1989~1991 과학재단 신진연구비에 의해 연구되었음.

In the previous application, a drastic simplification has been employed in coastlines. In this study, a little more realistic coastline is adapted to improve the wave guide in the main channel and in the northern embayment of the Yellow Sea. The qualitative improvement enables us to understand the dynamics in the Yellow Sea and to approach to a more realistic wave model. In addition, some numerical computations have been improved.

The present application is done for the same period as the previous one. As the surface winds are strong in winter, the channel model can be expected to be most applicable during the winter season. The January~April 1986 period is a particularly suitable time to make model calculations, as observations of currents and bottom pressure are available for comparison. These observations are the result of a three-month long field experiment in the eastern Yellow Sea designed to document and reveal the dynamics of wind-driven currents in the Yellow Sea(sueh, 1988).

Fig. 1 shows the geometry and bottom topography of the Yellow Sea and the locations of observation. The Yellow Sea is essentially a semienclosed north-south running shallow channel with a double shelf cross section. The study of long waves in semienclosed channels with flat bottoms dates back to the early 1900s(Taylor, 1921). In the late 1900s, long waves have been studied over bottom profiles characterized by a reverse slope encountered across submarine banks and trenches(Louis, 1978; Mysak *et al.*, 979; Mysak, 1980; Mysak and Willmott, 1981; Brink, 1983). However, the addition of Kelvin waves renders the circumstances in the Yellow Sea different. The purpose of the present study is to improve the existing basic theory and wave model over a double shelf.

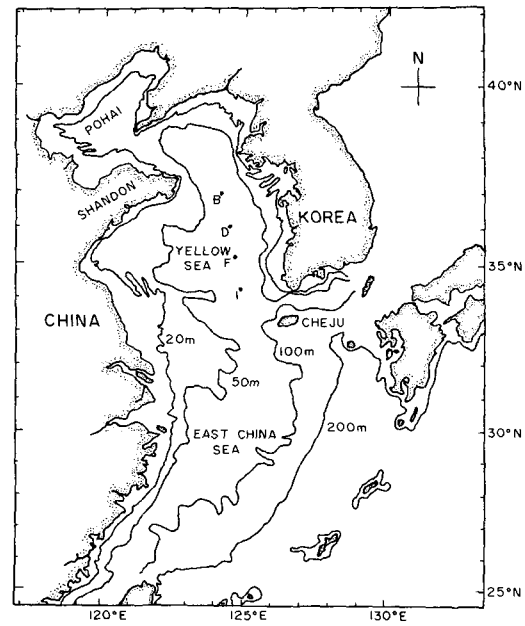

Fig. 1. Map of the Yellow Sea. Depths are in meters. Dots mark the locations of observation for the period of January 10 to April 12, 1986.

Theory

The process by which the wave model has been made is shown in Fig. 2. First step is to solve the free problem, in which bottom topography is incorporated. We have obtained the dispersion relation, from which the eigenvalues C_n(phase speeds here) are calculated, and the eigenfunctions F_n for a double shelf as shown in the Yellow Sea. In the next forced problem the first order wave equation is derived for a double shelf. By integration of wave equation, the wave function ϕ_n is solved. Geometry, frictional effect, and wind stress are incorporated in the wave equation. Finally, the eigenfunctions and wave functions are combined to get the sea level and current velocity.

1. First Order Wave Equation

For long shelf wave motions influenced by winds, small perturbations to a barotropic ocean satisfy the equation

$$(HP_{xt})_x+(rP_x)_x+fH_xP_y-\frac{f^2}{g}P_t=f(\tau^y{}_x-\tau^x{}_y) \qquad (1)$$

In this equation, x, y, t, P, g, f, r, H, τ^x and τ^y refer respectively to cross-shelf distance(eastward positive), alongshore distance(northward positive), time, perturbation pressure divided by mean water density, acceleration due to gravity, Coriolis parameter, bottom resistance coefficient, water depth, kinematic wind stresses in x and y direction at su-

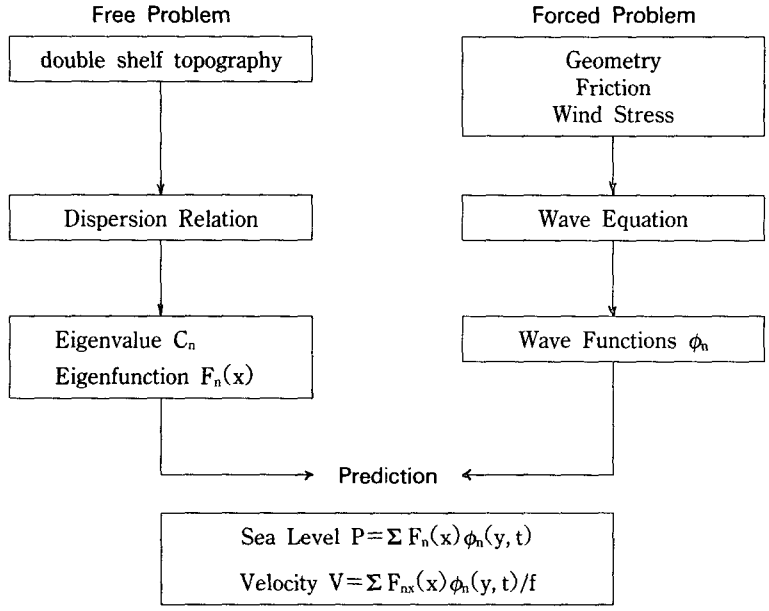

Fig. 2. Chart of the processes by which the wave model is made.

rface(the wind stresses divided by mean water density). Subscripts indicate derivatives.

Fig. 3 shows a schematic representation of the coordinates system and geometry of double shelves of linear depth profile, which is adapted for the Yellow Sea. The coordinate z refers to the vertical distance(upward positive). the origin of coordinates is set at the sea surface on the intersection of the trough and southern boundary. Shelf 1 and shelf 2 are placed in $-B_1 \le x \le B_2$, respectively. So, the linear bottom topography (H) can be set as follows:

$$H(x)=\begin{cases} H_1=H_0\dfrac{x+L_1}{L_1} \\ -B_1 \le x \le 0 \\ \text{in shelf 1(China shelf)} \\ H_2=-H_0\dfrac{x-L_2}{L_2} \\ 0 \le x \le B_2 \\ \text{in shelf 2(Korea shelf)} \end{cases} \qquad (2)$$

At the coastal boundaries, the no-flux bounary condition is applied, which means that the depth integrated offshore velocity vanishes(Pang, 1991, 1992). At the boundary between two shelves, the continuous boundary conditions of pressure and transverse velocity are applied, as follows:

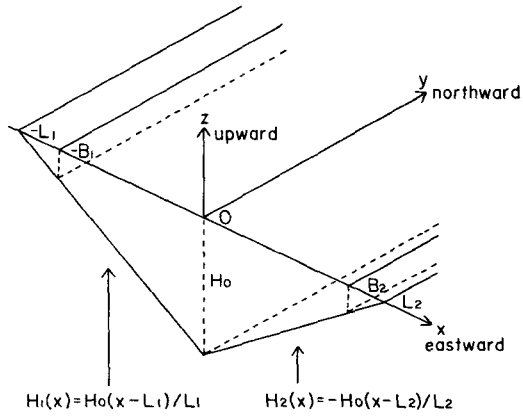

Fig. 3. Schematic representation of the coordinate system and the double shelf topography, which represents the Yellow Sea. The coordinates x, y and z refer to the cross-shelf(eastward positive), alongshore(northward positive), and vertical directions(upward positive), respectively. The greatest water depth is H_o. B_1 and B_2 are the locations of no-flux boundary where the water depth is 3 times the Ekman layer thickness(Mitchum and Clarke, 1986).

$$P_{1xt}+\frac{r}{h}p_{1x}+fP_{1y}=f\frac{Y}{h} \quad \text{at } x=-B_1 \qquad (3\text{-}1)$$

$$P_1=P_2 \quad \text{at } x=0 \qquad (3\text{-}2)$$

$$P_{1xt}+fP_{1y}=P_{2xt}+fP_{2y} \quad \text{at } x=0 \quad (3\text{-}3)$$

$$P_{2xt}+\frac{r}{h}p_{2x}+fP_{2y}=f\frac{Y}{h} \quad \text{at } x=B_2 \quad (3\text{-}6)$$

Setting $P(x,y,t)=\Sigma F_n(x)\phi(y,t)$ yields a Strum-Louville problem for frictionless eigenfunctions $F_n(x)$ as follows:

$$(HF_{nx})_x+\frac{f}{C_n}H_xF_n-\frac{f^2}{g}F_n=0 \quad (4)$$

$$F_{1nx}+\frac{f}{C_n}F_{1n}=0 \quad \text{at } x=-B_1 \quad (5\text{-}1)$$

$$F_{1n}=F_{2n} \quad \text{at } x=0 \quad (5\text{-}2)$$

$$F_{1nx}=F_{2nx} \quad \text{at } x=0 \quad (5\text{-}3)$$

$$F_{2nx}+\frac{f}{C_n}F_{2n}=0 \quad \text{at } x=B_2 \quad (5\text{-}4)$$

where F_{1n}, F_{2n}, C_n are eigenfunctions in shelves 1 and 2, the phase speed of nth mode, respectively.

Multiplying (1) by F_n and (4) by P_t and substracting them yields

$$F_n(HP_{xt})_x-P_t(HF_{nx})_x+(rP_x)_xF_n+fH_xF_n \times(P_y-\frac{P_t}{C_n})=fF_n(\tau^y{}_x-\tau^x{}_y) \quad (6)$$

By integrating (6) from $-B_1$ to B_2 with the boundary conditions (3) and (5), and expanding the pressure in terms of inviscid eigenfunctions with the orthogonality condition(Pang, 1992), it follows that, for mode n,

$$-\frac{\phi_{nt}}{C_n}+\phi_{ny}+\sum_{m=-\infty}^{\infty}a_{mn}\phi_m=b_{1n}\cdot\tau^y(-B_1) -b_{2n}\cdot\tau^y(B_2)+\frac{1}{r_n}\int_{-B_1}^{B_2}F_n\cdot(\tau^y{}_x-\tau^x{}_y)dx \quad (7)$$

where

$$a_{mn}=\frac{1}{f\cdot r_n}[(-r\cdot F_{mx}\cdot F_n)\Big|_{-B_1}^{B_2}+\int_{-B_1}^{B_2}(r\cdot F_{mx})_x\cdot F_n\,dx] \quad (8\text{-}1)$$

$$b_{1n}=\frac{F_n(-B_1)}{r_n} \quad (8\text{-}2)$$

$$b_{2n}=\frac{f_n(B_2)}{r_n} \quad (8\text{-}3)$$

$$r_n=(-H\cdot F_n^2)\Big|_{-B_1}^{B_2}+\int_{-B_1}^{B_2}H_x\cdot F_n^2\,dx \quad (8\text{-}4)$$

F_n's and ϕ_n's satisfy the boundary conditions and an infinite set of coupled first order wave equations, respectively. b_{1n} and b_{2n} are windcoupling coefficients at $x=-B_1$ and B_2, respectively. a_{nn} is a frictional decay coefficient and a_{mn} is a frictional coupling coefficient to mode m. The wave functions are coupled through friction. If there is no friction ($r=0$), $a_{mn}=0$ and the modes are decoupled. The reciprocal of $|a_{nn}|$ gives the decay distance for amplitude of the nth wave mode in the direction of wave propagation. For $r=3\times10^{-4}$*m/sec*, China shelf width $B_1=300$*km*, Korea shelf width $B_2=120$ *km*, the trough depth $H_0=100$*m*, coastal depth=20 *m*, the decay distance of Kelvin wave is 0(10,000 *km*) and that of the 1st continental shelf wave mode is 0(100*km*). Equation (7) can be solved by using the method of characteristics.

As shown in Pang(1991, 1992), there are two infinite sets of wave mode over a double shelf topography. We will use the positive(negative) n for the set of positive(negative) phase speed, which propagate southward(northward) along shelf 1 (2). For the Yellow Sea, the former(latter) will be called China(Korea) waves. The first modes(n=1, -1) are Kelvin waves and the other modes are continental shelf waves.

The first order wave equation (7) over a double shelf has wind stresses on both coastal boundaries and wind stress curl forcing across the shelf. Fig. 4 presents the comparison of the wind stress curl term with the wind stress term. The wind stress and wind stress curl are obtained from the atmospheric pressure charts. In calculating the wind stress curl, F_n is taken to be unity, representing the normalized value at coast, so that the wind stress curl term is over-estimated. By comparing, the wind stress curl is negligible except at a couple of times when the wind stress curl term shows a spike. The spikes are few in number. Thus, the effect of wind stress curl can be neglected as a forcing of shelf in the Yellow Sea.

2. Numerical Method of Characteristics

If we limit the problem to a finite number of modes, 2j, (7) can be written as follows:

$$-\frac{\phi_{nt}}{C_n}+\phi_{ny}+a_{nn}\phi_n=G_n(y,t) \quad (9)$$

where the forcing function $G_n(y,t)$ is defined as follows:

$$G_n(y,t)=-\sum_{-j(j\neq0)}^{j}a_{mn}\phi_m+b_{1n}\cdot\tau^y(-B_1)-b_{2n}\cdot\tau^y(B_2) \quad \text{except n} +\frac{1}{r_n}\int_{-B_1}^{B_2}F_n\cdot(\frac{d\tau^y}{dx}-\frac{d\tau^x}{dy})dx \quad (10)$$

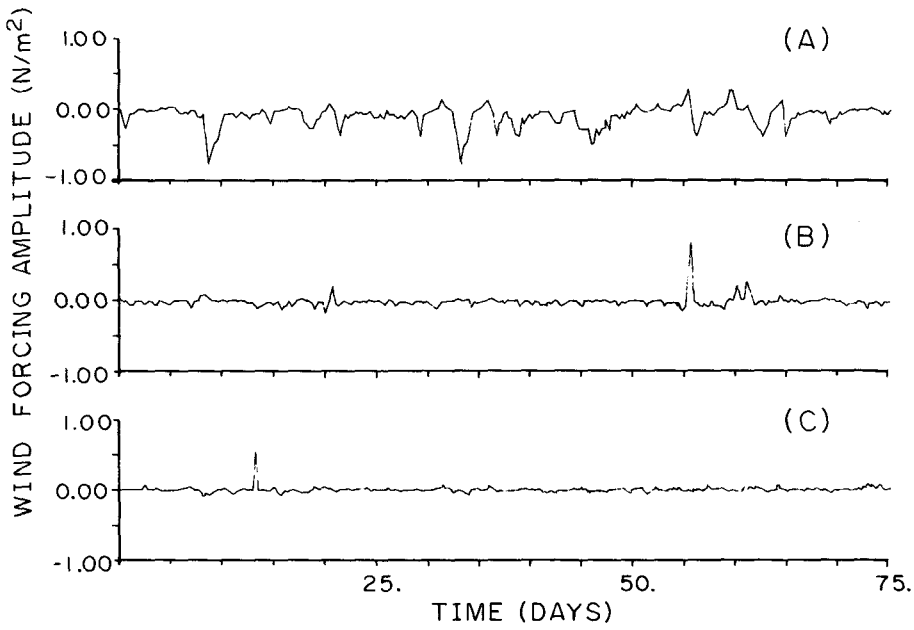

Fig. 4. Comparison of the wind stress curl terms by (B) north-south component and (C) east-west component with (A) the wind stress term.

Along the characteristics defined by $Y_{nt}=-C_n(Y_n[t])$, (9) yields

$$\phi_{nt}-C_n a_{nn}\phi_n=-C_n G_n(Y_n[t],t) \tag{11}$$

Multiplying (11) by the integration factor as

$$E(t)=\exp[\int_0^t\{-C_n\}\{Y_n(t^*)\}a_{nn}\{Y_n(t^*)\}dt^*]$$

and integrating from $t-\delta t$ to t gives

$$\phi_n\{Y_n(t),t\}=\phi_n\{Y_n(t-\delta t),t-\delta t\}E(t-\delta t)/E(t)$$
$$+\int_0^t[-C_n\{Y_n(t^*)\}G_n\{Y_n(t^*),t^*\}a_{nn}\{Y_n(t^*)\}dt^*] \tag{12}$$

wheter $Y_n(t^*)=Y_n(t)+\int_{t^*}C_n\{Y_n(t')\}dt'$.

Using the trapezoid rule to evaluate the integral in (12) gives the following difference formula relating $\phi_n\{Y_n(t),t)\}$ to $\phi_n\{Y_n(t-\delta t),t-\delta t\}$.

$$\begin{aligned}\phi_n\{Y_n(t),t\}&=\phi_n\{Y_n(t-\delta t),t-\delta t\}\\&\times\exp[(\delta t/2)\cdot[C_n\{Y_n(t)\}\cdot a_{nn}\{Y_n(t)\}\\&+C_n\{Y_n(t-\delta_t)\}\cdot a_{nn}\{Y_n(t-\delta t)\}]]\\&-(\delta t/2)\cdot C_n\{Y_n(t)\}\cdot G_n\{Y_n(t),t\}\\&-(\delta t/2)\cdot C_n\{Y_n(t-\delta t)\}G_n\{Y_n(t-\delta t),t-\delta t\}\\&\times\exp[(\delta t/2)\cdot[C_n\{(Y_n(t)\}\cdot a_{nn}\{Y_n(t)\}\\&+C_n\{Y_n(t-\delta t)\}\cdot a_{nn}\{Y_n(t-\delta t)\}]]\end{aligned} \tag{13}$$

where $Y_n(t-\delta t)=Y_n(t)+(\delta t/2)\cdot[C_n\{Y_n(t)\}+C_n\{Y_n(t-\delta t)\}]$.

Using the equation (10) enables (13) to be written as the matrix equation as follows:

$$\Gamma\cdot[I-(\delta t/2)K]=Q$$

where Γ is a row vector with the element $\phi_n(Y,t)$ and I is the identity matrix with j by j. The matrix K is given by

$$\begin{cases}0 & \text{when } m=n\\ C_n\{Y_n(t)\}\cdot a_{mn} & \text{when } m\neq n\end{cases}$$

and Q is a row vector given by

$$\begin{aligned}q_n=&-(\delta t/2)C_n\{Y_n(t)\}[b_{1n}\tau^y(-B_1)-b_{2n}\tau^y(B_2)\\&-\frac{1}{r_n}\int_{-B_1}^{B_2}F_n(\tau^y{}_x-\tau^x{}_y)dx]_{t=t}\\&+\phi_n\{Y_n(t-\delta t),t-\delta t\}\\&\times\exp[(\delta t/2)[C_n\{Y_n(t)\}a_{nn}\{Y_n(t)\}\\&+C_n\{Y_n(t-\delta t)\}a_{nn}\{Y_n(t-\delta t)\}]]\\&-(\delta t/2)\cdot C_n\{Y_n(t-\delta t)\}\cdot G_n\{Y_n(t-\delta t),t-\delta t\\&\times\exp[(\delta t/2)\cdot[C_n\{Y_n(t)\}\cdot a_{nn}\{Y_n(t)\}\\&+C_n\{Y_n(t-\delta t)\}\cdot a_{nn}\{Y_n(t-\delta t)\}]]\end{aligned} \tag{14}$$

With the restriction that $\varepsilon=(K\delta t/2)^2=(\delta t)^2 j(K_{max})^2/4\ll 1$, we have within a small ereor ε

$$[I-(\delta t/2)K]^{-1}=[I+(\delta t/2)K].$$

Consequently, the solution for ϕ_n is

$$\Gamma=Q\cdot[I+(\delta t/2)K]. \tag{15}$$

In addition, δt must be small enough so that there is the same resolution in t as in y and aliasing is

prevented.

Since, over a double shelf, there are two infinite wave sets propagating in opposite directions, we need two boundary conditions. Fig. 5 shows (A) an analytical solution and (B) a numerical solution of the first two modes over a double shelf(300~120 *km*) channel of 500*km* length shown in Fig. 6, calculated by a simple sinusoidal wind forcing $\tau^y=\tau_0\cdot\cos(ly+wt)$. The values of τ_0, ℓ, and w are, respectively, $10^{-1}N/m^2$, $10^{-6}m^{-1}$, and $10^{-5}sec^{-1}$. Fig. 6 shows the model channel of straight coastlines in replacement of the Yellow Sea, which is used in the previous application. The solid curves represent the time series of the wave function(ϕ_{-1}) propagating in the (+) y direction. So, its amplitude increases from the southern boundary(transection a at y=0*km*) where it is set to be zero to the northern boundary(transection b at y=500*km*). On the other hand, the dashed curves represent the time series of the wave function(ϕ_1) propagating in the (−) y direction. So, its amplitude increases from the northern boundary where it is set to be zero to the southern boundary. The analytical and numerical solutions show discrepancies only at the beginning. The initial difference is due to the fact that the analytical solution has only boundary conditions while the numerical solution has both boundary and initial conditions. Initially, sea level fluctuation is set to zero everywhere for the numerical solution. The duration over which the initial difference persists depends upon the phase speed C_n and is the time for the waves to travel the channel($t=-y/C_n$ for waves propagating [+] y direction and $t=(500-y)/C_n$ for waves propagating [−] y direction). After the initial period, solutions are affected only by the boundary conditions and agree with each other, which implies that the numerical method works.

Fig. 7 and Fig. 8 show, respectively, the fluctuations in sea level and alongshore velocity along the Korea coast, calculated by the same wind foring. The 3 pannels shown in the figures represent the model results calculated with inclusion of the first (A) 2, (B) 4, and (C) 6 wave modes. As wave function, the amplitude of sea level and alongshore velocity increases from the southern boundary to the northern boundary along the Korea coast. The Kelvin wave mode makes a substantial contribution

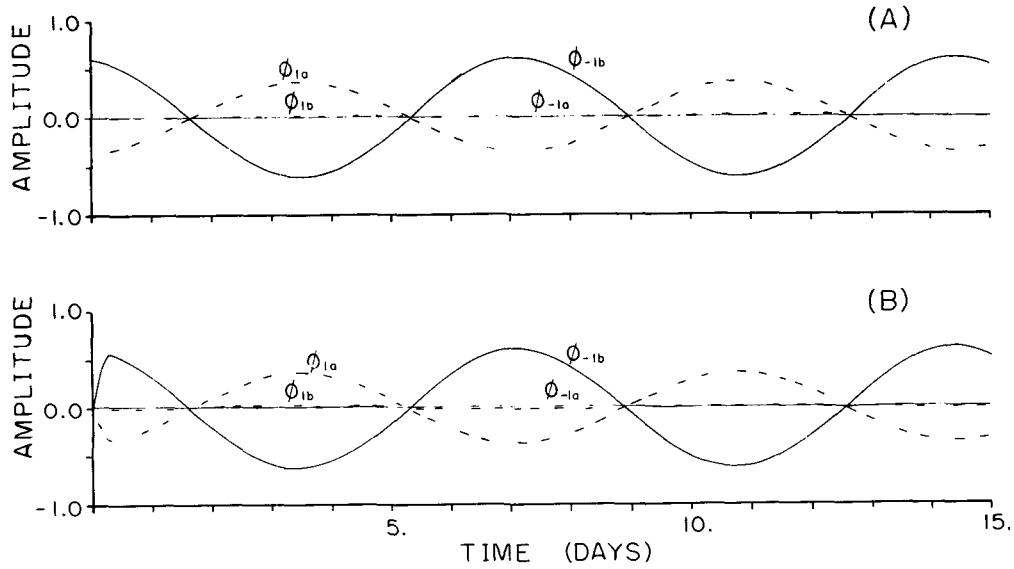

Fig. 5. (A) analytical and (B) numerical solutions of the first two wave functions: ϕ_1(dashed lines) and ϕ_{-1}(solid lines). The amplitude is non dimensional. A northward(southward) propagating wave function $\phi_{-1}(\phi_1)$ is amplified from the transection a (b) to the transection b (a) shown in Fig. 6. Numerical solutions are set to zero initially.

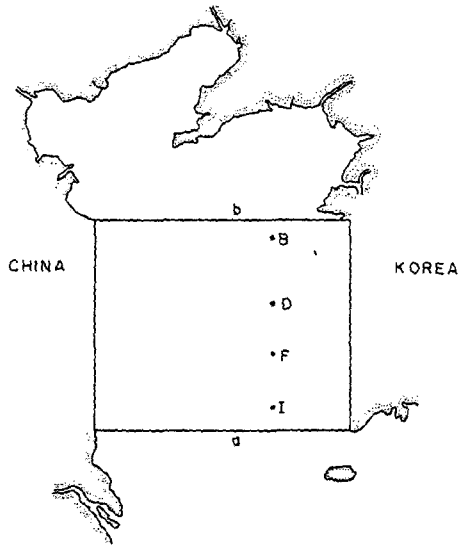

Fig. 6. A schematic representation of the insertion of the model channel in replacement of the Yellow Sea. The transections a and b mark the ends of the channel. B, D, F, and I, which lie along the model trough, are the locations of observation for the period of January~April, 1986.

(about 80%) to sea level fluctuations. After the first 4 modes are included, there is no perceptible difference in the solutions. The sea levels calculated with the inclusion of the first 4 modes are thus a good approximation to the total solutions. It means that sea level fluctuations are due mainly to the existence of Kelvin waves. However, Fig. 8 shows that Kelvin wave modes contribute almost nothing to alongshore velocity. Velocity is due mainly to the presence of continental shelf wave modes, among which the 1st modes contribute the most.

Modelling of the Yellow Sea

We applied the wave theory to reproduce the observed sea level and velocity fluctuations driven by wind during the period of January 13 to March 29, 1986. The application is performed by the integration of (9) along characteristics, with the bottom resistance coefficient(r) of $3\times10^{-4}m/sec$. As in the

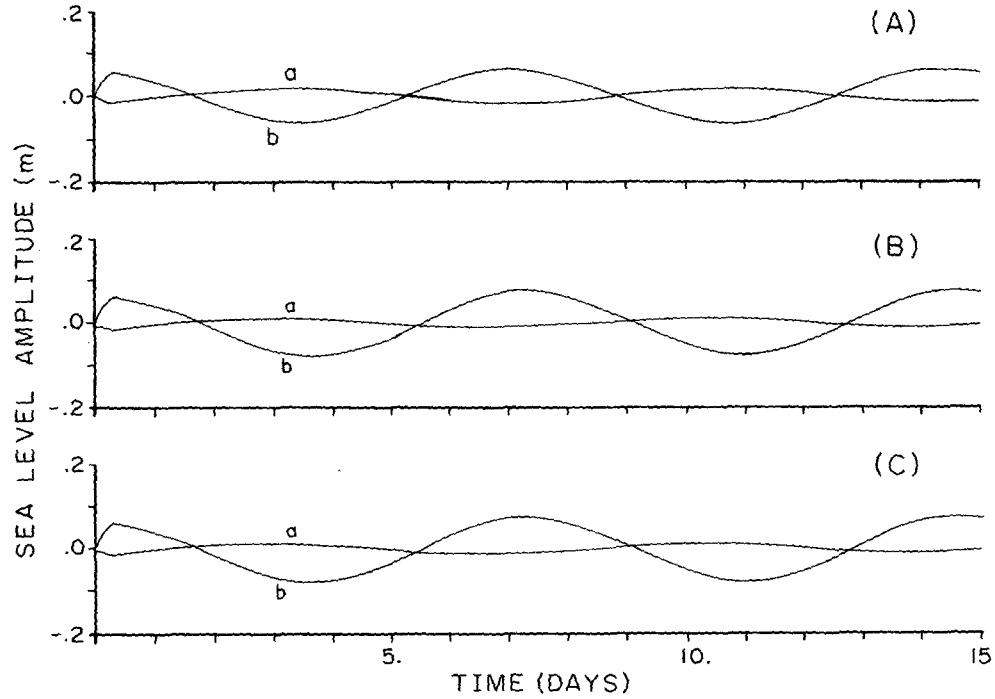

Fig. 7. Time series of calculated sea level fluctuations along Korea coast with inclusion of the first (A) 2, (B) 4, (C) 6 wave modes, driven by a simple sinusoidal wind forcing $\tau^y=\tau_0\cdot\cos(\ell_y+\omega t)$, where τ_0, ℓ, and ω are 10^{-1} Netwton/m^2, 10^{-6} m^{-1}, and 10^{-5} sec^{-1}, respectively.

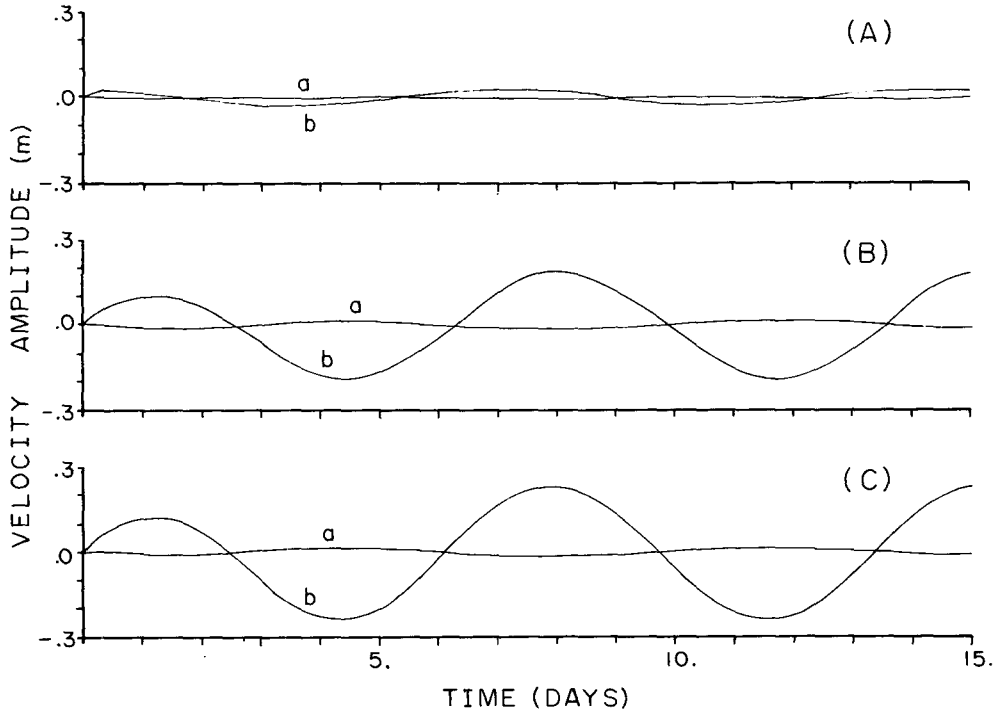

Fig. 8. Time series of calculated velocity fluctuations along Korea coast with inclusion of the first (A) 2, (B) 4, (C) 6 wave modes, driven by a simple sinusoidal wind forcing $\tau^y=\tau_0 \cdot \cos(\ell_y+\omega t)$, where τ_0, ℓ, and ω are 10^{-1} Newton/m^2, 10^{-6} m^{-1}, and 10^{-5} sec^{-1}, respectively.

previous research(Pang, 1987; Hsueh and Pang, 1989), the Yellow Sea is divided into two parts: the main region, which is bounded to the south by the tip of Korean Peninsula and to the north by the Shandon Peninsula, and the northern boundary region, which is the embayment north of the Shandon Peninsula. The north-south separation of the main region is set to be 500*km*, roughly the curved alongshore distance from the end of the Korean Peninsula to Inchon on the Korea side and from Qingdao on the southern coast of Shandon Peninsula to a coastal point just north of the Changjiang mouth on the China side.

Fig. 9 depicts schematically the placement of the model channel in the geographical setting of the Yellow Sea. For the main region, the straight coast line used previously(Fig. 6) is rather crude in the incorporation of wave guide effects. In this paper, a little more realistic coast line is chosen(Fig. 9). The choice has improved the representative model cross section, which is difficult by a substantial alo-

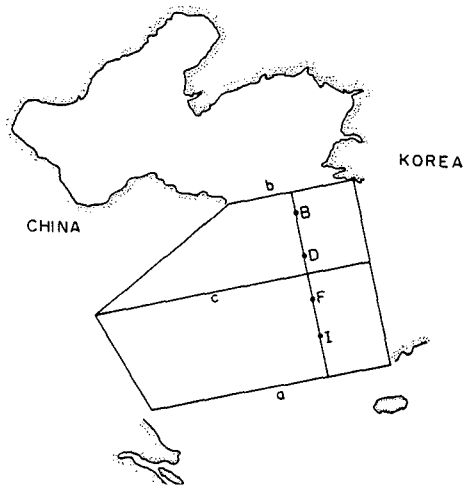

Fig. 9. A schematic representation of a little more realistic model domain in replacement of the Yellow Sea. The transections a and b mark the ends of the channel and the transection c marks the widest shelf width. B, D, F, and I, which lie along the model trough, are the locations of observation for the period of January~April, 1986.

ngshore variation of the cross-sectional topography in reality. The cross-sectional shelf widths(China Shelf-Korea Shelf) along the transections of a, c, and b are 300*km*~120*km*, 400*km*~120*km*, and 120 *km*~120*km*, respectively.

Since the decay distance in the direction of wave propagation is on the order of 10,000*km* for Kelvin waves and of 100*km* for continental shelf waves, the Kelvin wave propagating northward along the Korea shelf is expected to be transmitted nearly intact through the northern boundary region and to propagate southward along the China shelf, while there will be no such direct supply of energy to the continental shelf waves on the China shelf. The almost east-west running northern coast of Shandon Peninsula also renders ineffective for the generation of shelf waves by winds in winter, which are primarily from the north.

The transmission of Kelvin wave in the northern boundary region is accomplished by replacing a 500 *km*-long single shelf waveguide. The length of transitional waveguide is chosen to assure a reasonable representation of the phase relation and of the amount of attenuation expected around the northern end of the Yellow Sea, largely along the 50*m* isobath. Offshore from the waveguide, a body of water of constant depth of 100*m* is assumed. Despite the allowance for the transmission of Kelvin wave from the Korea shelf to the China shelf, the model is basically one of an infinitely long channel, which is empirical and crude in its incorporation of end effects. In the northern closed embayment, evanescent Poincaré waves can still be generated, resulting in a reduction in the energy level of Kelvin wave before it reaches the China side(LeBlond and Mysak, 1980). The amount of reduction is a function of coastal geometry and is currently unknwon.

The surface winds for this experimental period have been successfully estimated from the surface pressure charts(Hsueh and Tinsman, 1987). These winds can be expected to have very large correlation distance(Hsueh and Romea, 1983). For the purpose of driving the simple model, the geostrophic winds calculated from the surface pressure fields will be used. The wind stress have been computed from the wind velocity using a constant drag coefficient C_d of 1.5×10^{-3}. The estimated wind stress curl term is smaller than the wind stress contributions by a couple of orders of magnitude. Thus, winds are assumed spatially uniform and equal to those calculated at 125°E, 35°N, as shown in Fig. 10.

The method of characteristics is shown previously. It is basically the same idea as that found in Clarke and VanGorder(1986), however, the algorithm of integration process is different in time increment to accomodate wave propagations to the north and south. The integration process is shown in Fig. 11. The x-axis represents the distance of

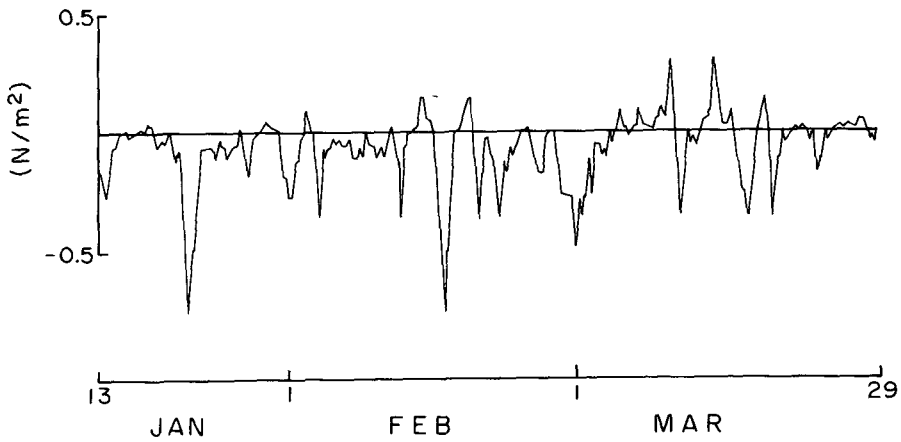

Fig. 10. Alongshore wind stresses calculated from the pressure chart during January 13 to March 29, 1986.

wave guide counterclockwisely from and back to the southern boundary(transection a in Fig. 9) through the northern boundary region. The y-axis represents the time process for the slowest wave mode to propagate around the Yellow Sea along the wave guide. When it comes back to the southern boundary, we get the complete soultion. It has been shown that the wind-driven sea level response is probably at a minimum at the end of the Korean Peninsula, where deep open water is encountered. It thus appears that a no-incoming wave condition ($\phi_n=0$ for $n<0$) may be safely imposed across

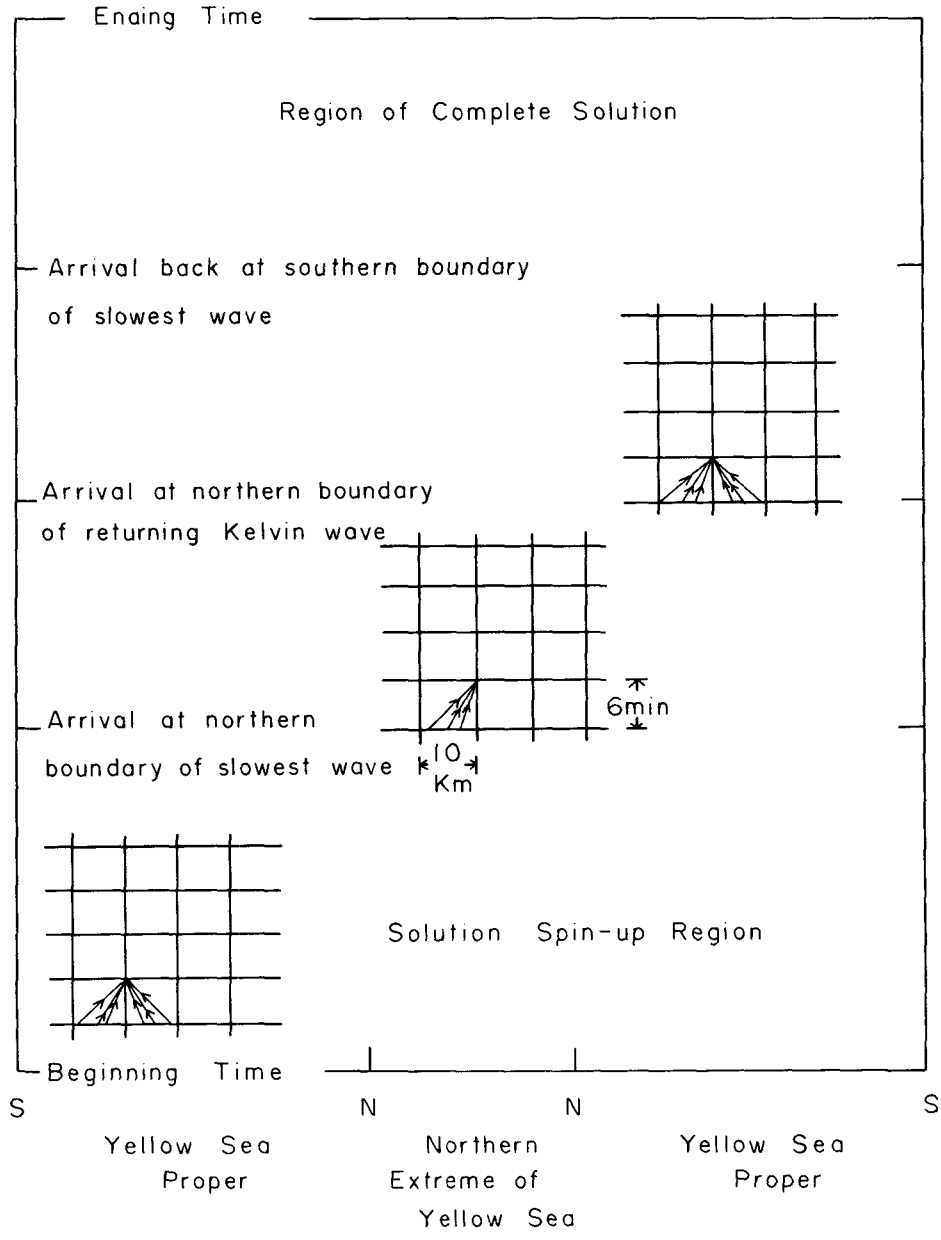

Fig. 11. Schmatic representation of numerical calculation along characteristics. Horizontal axis represents the wave propagation route counterclockwisely in the Yellow Sea, from and back to the southern boundary through the northern embayment. Vertical axis represents the arrival time of waves.

the Yellow Sea along the southern boundary. In the northern boundary region, only Kelvin wave is allowed to propagate from the main region, so $\phi_n=0$ for all $n<0$ except $n=1$. The integration is made at Δt increment of 6 minutes and Δy of 10*km*. The ocean is assumed to be initially at rest. Comparison of current velocities is made at current meter mooring locations of which the approximately corresponding positions in the model are marked in Fig. 9.

Application and Results

Fig. 12 shows the comparison of the sea level fluctuations of observations(solid line), model results with a straight coast lines(dotted line), and model results with a little more realistic coast lines (dashed line) at stations B and D. Fig. 13 shows the comparison of the velocity fluctuations of the same way at stations B, D, F, and I. Despite the drastic simplification employed, the model appears to reproduce qualitatively main features of the observation, particularly the reproduction of upwind flows in the Yellow Sea trough that have been observed to be driven by north-south setup in coastal sea level(Hsueh, 1988). The sea level fall due to the north wind pulses is clearly reproduced. The model output tracks particularly well the measure-

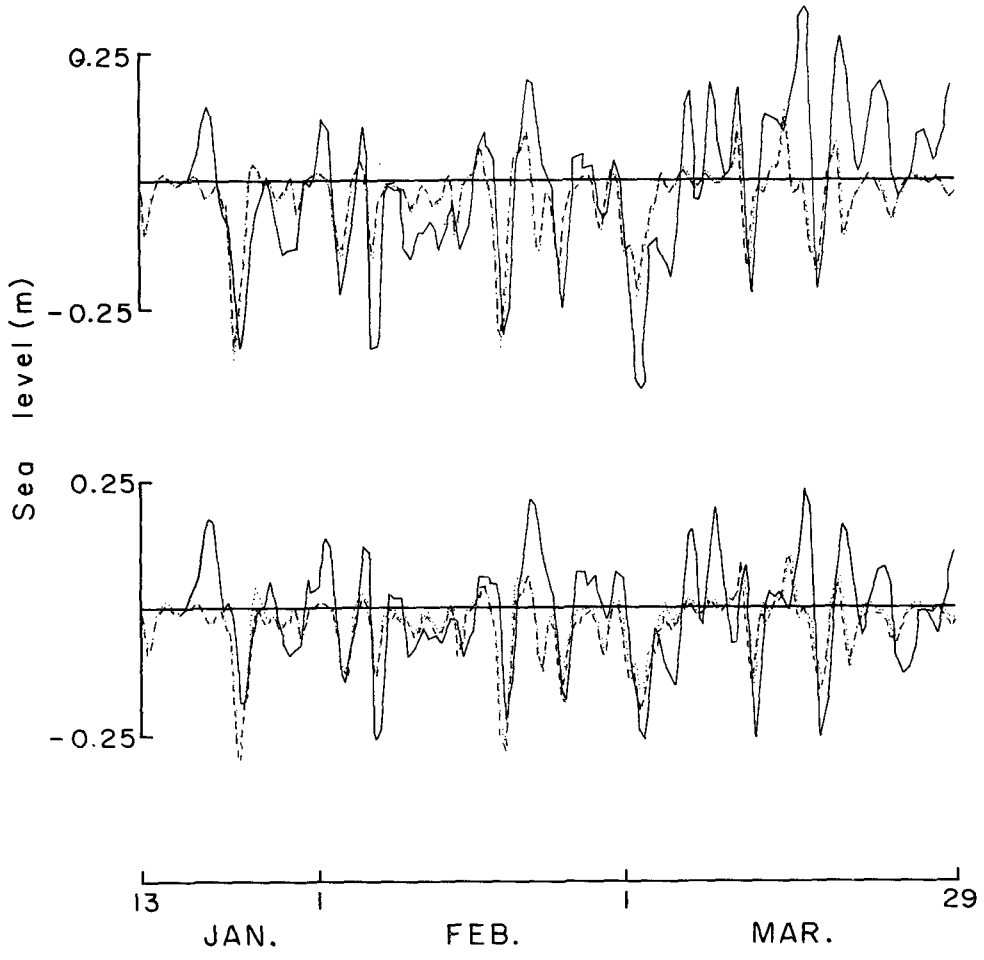

Fig. 12. Comparison of sea level fluctuations of observations(solid line), model results with a straight coast lines (dotted line), and model results with a little more realistic coast lines(dashed line) at stations B(upper pannel) and D(lower pannel) during January 13 to March 29, 1986.

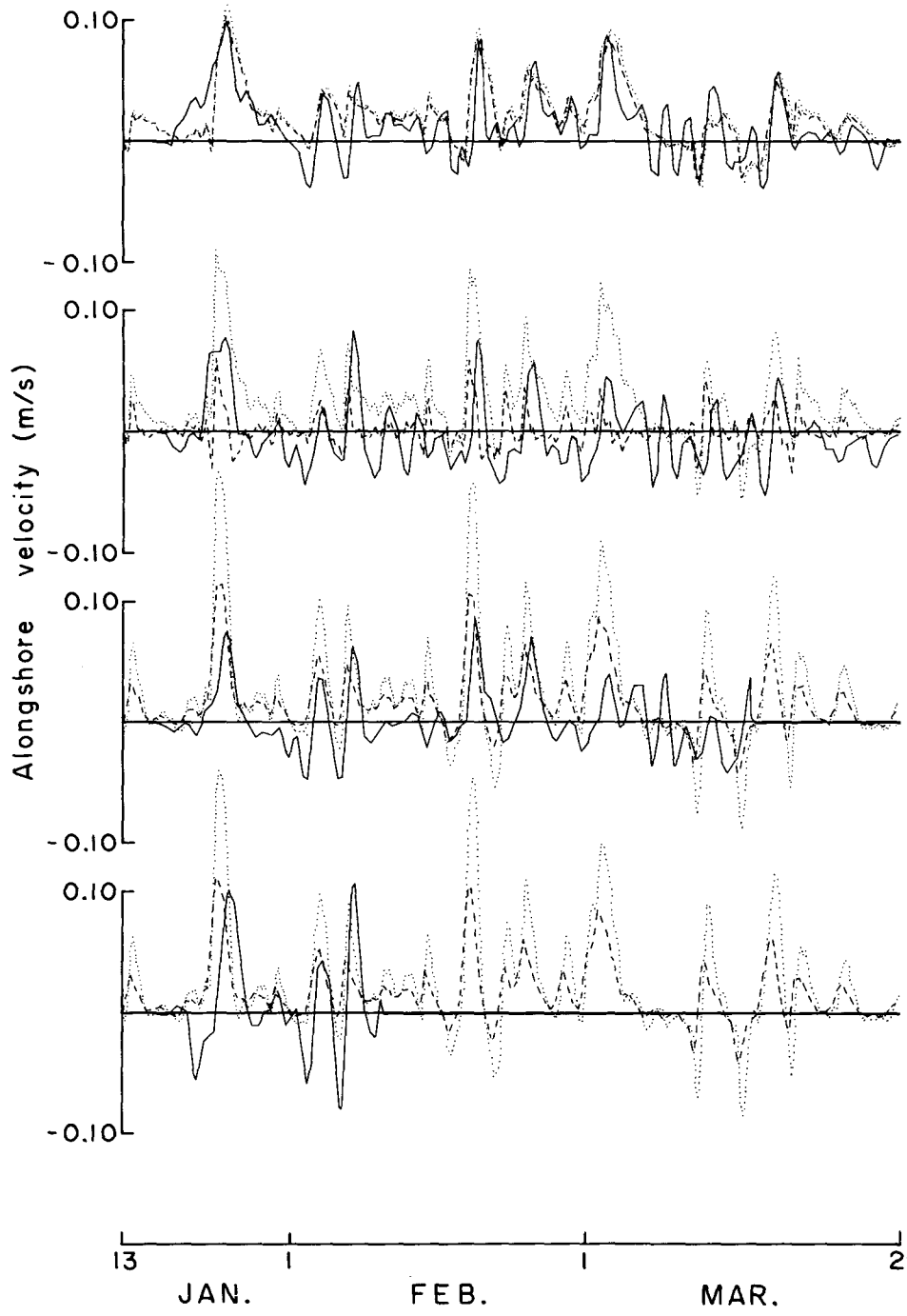

Fig. 13. Comparison of velocity fluctuations of observations(solid line), model results with a straight coast lines (dotted line), and model results with a little more realistic coast lines(dashed line) at stations B, D, F, and I from the top pannel to the bottom pannel during January 13 to March 29, 1986.

ments at B and D. The sea level difference between stations B and D is of special significance to the development of the upwind flow in the trough.

The change of coast lines improves little the model reproductions of sea level, because sea levels are mainly determined by the Kelvin waves and the Kelvin waves are affected little by the change of bottom slope in China shelf. Both of the model reproductions of sea level are by and large good in phase but not so good in amplitude. This is probably due to the geostrophic wind calculated from the pressure chart. The geostrophically calculated wind stress is likely to be accurate in phase but not in amplitude. The sea level reproduction is also sensitive to the northern boundary because of the transmission of Kelvin wave. For better sea level reproduction on the Yellow Sea area, we need eventually some modifications in modelling the northern boundary region.

The change of bottom slope does not improve the alongshore velocity in the northern part along the Yellow Sea trough. However, both models work quite well, as we can see that at station B for alongshore velocity. The northern part along the Yellow Sea trough may be the best place to see how well the model work, since the flow is least affected by other dynamics. The area is far from the coasts and boundary. The good agreement of the alongshore velocity at station B indicates that the wave model works fine basically for a double shelf topography and that the assumptions adapted are acceptable. One assumption is no incoming wave energy from the southern boundary. It turns out to be fine for velocity, however, not good for sea level. The tidal observations at the tip of Korean Peninsula show singnificant sea level fluctuations. It indicates some incoming wave energies in the form of Kelvin waves. Another assumption is no incoming continental shelf waves from the northern boundary. It is based on the longer coastline of northern embayment than the decay distance of shelf waves and on the ineffective coastal direction of Shandon Peninsula to generate shelf waves by the prevailing north-south winds in winter.

The variations of bottom topography over the China shelf affect the China continental shelf waves and so the velocity near the southern boundary. The discrepancies of velocity shown in the model results with straight coastlines near the southern boundary have been reduced by using a more realistic coast line. More improvement in the southern part implies that the waters near the southern part is influenced more by China shelf waves. Because China shelf waves are fully developed there while Korea shelf waves are not sufficiently developed yet.

The current velocity from the models is downwind along coasts(not shown), which agrees with Park(1986). The basic structure of downwind flows along the coasts and upwind flows along the trough supports the seasonal circulations driven by monsoon winds in the Yellow Sea(Pang *et al.*, 1992), which is shown in Fig. 14.

Discussion and Conclusion

The first order wave equation over a douple shelf has wind stresses on both coastal boundaries and wind stress curl forcing across the shelf. However, the effect of wind stress curl can be neglected as a forcing of shelf waves in the Yellow Sea. (Wind stress curl has an effect in such a way that a positive curl amplifies the wave functions of Korea modes, which propagate northward along the shelf 2 with negative phase speeds.)

The decay distance of Kelvin waves is much greater than that of continental shelf waves. therefore, Kelvin waves are transmitted nearly intact through the northern embayment while continental shelf waves are not. It suggests that the northern embayment of the Yellow Sea is necessary to be modelled for sea level hindcast, but not for velocity hindcast. Fig. 15 shows the comparison of (A) sea levels and (B) velocities, which are obtained with and without the modeled northern boundary region. By modelling the northern boundary region, sea level reproduction has been affected largely while velocity reproduction has not.

Using a little more realistic coastalline, the wave model hindcast has been improved for current ve-

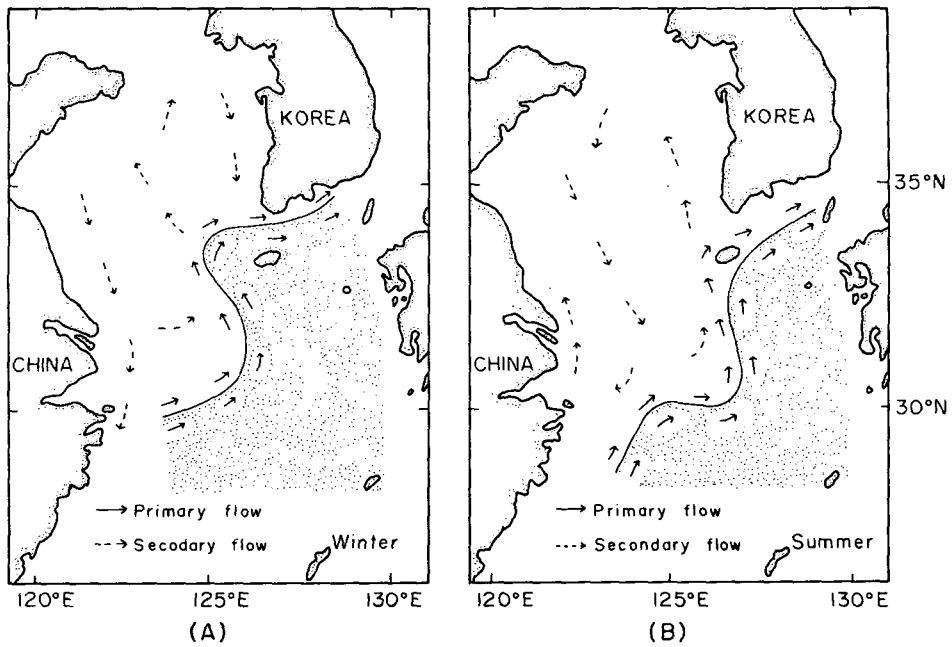

Fig. 14. A schematic circulation diagram in the Yellow Sea and the East China Sea (A) in winter and (B) in summer, based on the two circulations: primary one driven by Kuroshio transport and secondary one driven by monsoon winds. (from Pang *et al.*, 1992)

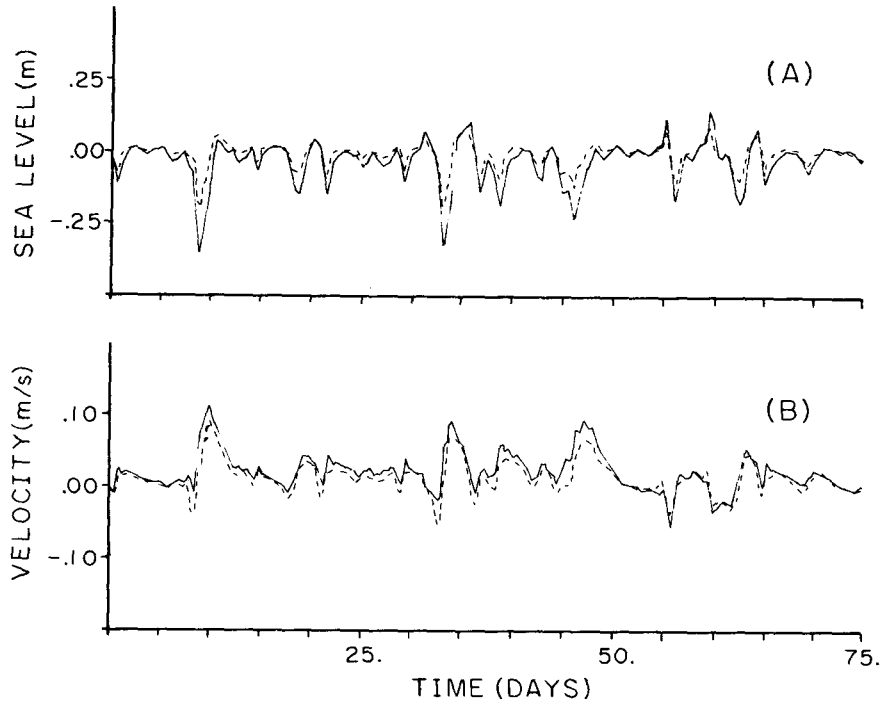

Fig. 15. Comparison of (A) sea levels and (B) velocities at station B, obtained with(solid line) and without (dashed line) the modelled northern boundary region.

locity, but hardly for sea level. It means that Kelvin waves, which mainly determine sea levels, are affected little by the change of bottom slope. For a better hindcast of sea level, input energy of Kelvin waves transmitted from the East China Sea is needed.

Sea level difference between stations B and D is of special significance to the development of the upwind flow in the trough. The inclination of sea level has been observed to be driven by north-south setup(Hsueh, 1988), and the sea level fall due to the north wind pulses is clearly reproduced.

The basic structure of downwind flow along the coasts and upwind flow along the trough supports the seasonal circulations driven by monsoon winds.

Although the wave model has been improved so far, it should be improved more for better reproductions, specially in modelling the northern embayment. It is a future task, however, we understand that the long-period fluctuations of sea level and alongshore velocity in the Yellow Sea are basically due to the large scale ocean response driven by winds.

References

Brink, N. H. and J. S. Allen. 1978. On the effect of bottom friction on barotropic motion over the continental shelf. J. Phys. Oceanogr., 8, 919~922.

Brink, N. H. and J. S. Allen. 1983. Low-frequency free wave and wind-driven motions over a submarine bank. J. Phys. Oceanogr., 13, 103~116.

Clarke, A. J. and S. Van Gorder. 1986. A method for estimating wind-driven frictional time-dependent, stratified shelf and slope water flow. J. Phys. Oceanogr., 16, 1013~1028.

Gill, A. E. and E. H. Schumann. 1974. The generation of long shelf waves by the wind. J. Phys. Oceanogr., 4, 83~90.

Hsueh, Y. 1988. Recent Current Observations in the eastern Yellow Sea. J. Geophys. Res., 93, 6875~6844.

Hsueh, Y. and I. C. Pang. 1989. Coastally trapped long waves in the Yellow Sea. J. Phys. Oceanogr., 19(5), 612~625.

Hsueh, Y. and R. D. Romea. 1983. Wintertime winds and coastal sea-level fluctuations in the Northeast China Sea. Part 1: Observations. J. Phys. Oceanogr., 13, 2091~2106.

Hsueh, Y. and J. H. Tinsman III. 1987. A Comparison between Geostrophic and Observed Winds at a Japan Meteorological Agency buoy in the east China Sea. J. Oceanogr. Soc. Japan, 43, 251~257.

LeBlond, P. H. and L. A. Mysak. 1980. Waves in the Oceans. Elsevier, 602pp.

Louis, J. P. 1978. Low-frequency edge waves over a trench-ridge topography adjoining a straight coastline. Geophys. Astrophys. Fluid Mech., 55, 113~127.

Mitchum, G. T. and A. J. Clarke. 1986. The frictional nearshore response to forcing by synoptic scale winds. J. Phys. Oceanogr., 16, 934~946.

Mysak, L. A., P. H. LeBlond and W. J. Emery. 1979. Trench waves. J. Phys. Oceanogr., 9, 1001~1013.

Mysak, L. A. 1980. Recent advences in shelf wave dynamics. Rev. Geophys. Space Phys., 18, 211~241.

Mysak, L. A. and A. J. Willmott. 1981. Forced trench waves. J. Phys. Oceanogr., 11, 1481~1502.

Pang, I. C. 1987. Theory of coastally trapped waves and its application to the Yellow Sea. Ph. D. Dissertation, Florida State University, 128pp.

Pang, I. C. 1991. Coastally trapped waves over a double shelf topography (I): Free waves with exponential topography. Bull. Korean Fisher. Soc., 24(6), 428~436.

Pang, I. C. 1992. Coastally trapped waves over a double shelf topography (II): Free waves with linear topography. Bull. Korean Fisher. Accepted.

Pang, I. C., H. K. Rho and T. H. Kim. 1992. Seasonal Variations of Water Mass Distributions and their Causes in the Yellow Sea, the East China Sea, and the Adjacent Seas of Cheju Island. Bull. Korean Fisher. Soc., 25(2), 151~163.

Park, Y. H. 1986. A simple Theoretical Model for the Up-wind flow in the Southern Yellow Sea.

J. Oceanogr. Soc. Korea, 21, 203~210.

Taylor, G. I. 1921. Tidal Oscillations in gulfs and rectangular basins. Proc. Lond. Math. Soc., 2 (20), 148~181.

Received October 2, 1992
Accepted November 7, 1992

양향성 대륙붕의 대륙붕파 (III): 강제파와 황해에서의 바람에 의한 해수순환

방 익 찬
제주대학교 해양학과

양향성 대륙붕에서 1차 파동방정식은 양 해안경계에서의 바람응력과, 대륙붕폭에 걸친 바람응력의 회전효과를 갖는다. 황해에서 바람응력 회전효과는 대륙붕파를 발생시키는 힘으로서 무시될 수 있다. 켈빈파는 대륙붕파보다 약화될 때까지의 거리가 매우 크기 때문에 황해 북쪽만(灣)을 거의 약화되지 않고 통과할 수 있다. 파동특성을 따라 적분하는 수치방법은 반대방향으로 전파되는 파동을 수용하기 위해 조절되었다.

보다 실제와 가까운 해안선을 사용한 결과, 모델재생이 해류에서는 개선되었으나 해수면에서는 거의 개선되지 않았다. 이것은 해수면을 주로 결정하는 켈빈파가 해저지형의 변화에 영향을 극히 적게 받음을 의미한다. 보다 개선된 해수면 재생을 위해서는 동지나해에서 황해로 전파되는 켈빈파의 에너지를 알 필요가 있다. 해안을 따른 순풍류와 골을 따른 역풍류의 기본구조는 계절풍에 의해 발생하는 황해의 계절순환을 뒷받침한다.